In-situ compositional and structural analysis of plastic solar cells

van Duren, J.K.J.; Morrissey, F.; Leewis, C.M.; Kivits, K.P.H.; van IJzendoorn, L.J.; Rispens, M.T; Hummelen, Jan; Janssen, R.A.J.

Published in:
Advanced Functional Materials

DOI:
10.1002/1616-3028(20021016)12:10<665::AID-ADFM665>3.0.CO;2-J

Publication date:
2002

In-Situ Compositional and Structural Analysis of Plastic Solar Cells**

By *Jeroen K. J. van Duren*, *Joachim Loos*, *Francis Morrissey*, *Christian M. Leewis*, *Koen P. H. Kivits*, *Leo J. van IJzendoorn*, *Minze T. Rispens*, *Jan C. Hummelen*, and *René A. J. Janssen**

Bulk-heterojunction photovoltaic cells consisting of a photoactive layer of poly[2-methoxy-5-(3′,7′-dimethyloctyloxy)-1,4-phenylenevinylene] (MDMO-PPV) and a C_{60} derivative, (1-(3-methoxycarbonyl)propyl-1-phenyl-[6,6]-methanofullerene), (PCBM), sandwiched between an indium tin oxide (ITO) anode covered with poly(ethylene dioxythiophene):poly(styrene sulfonate) (PEDOT:PSS), and an aluminum cathode have been analyzed using transmission electron microscopy (TEM) and cryogenic Rutherford backscattering spectrometry (RBS) to assess the structural and elemental composition of these devices. TEM of cross sections of fully processed photovoltaic cells, prepared using a focused ion beam, provide a clear view of the individual layers and their interfaces. RBS shows that during preparation diffusion of indium into the PEDOT:PSS occurs while the diffusion of aluminum into the polymer layers is negligible. An iodinated C_{60} derivative (I-PCBM) was used to determine the concentration profile of this derivative in the vertical direction of a 100 nm active layer.

1. Introduction

Polymer light-emitting diodes and polymer photovoltaic cells typically consist of a ≈100 nm thick active layer, sandwiched between a transparent front electrode and a metal back electrode.[1] Such single layer devices are often augmented with additional layers for further optimizing the performance or lifetime of the devices. Such additional layers are introduced to enhance charge transport, promote the injection or collection of charges, or control the zone where recombination (in LEDs) or generation (in solar cells) of charge carriers occurs. For polymer devices, processing conditions, the thickness and roughness of the layers, the integrity of the interfaces, the chemical composition, and their morphological structure have been identified as important parameters for the device performance. For example, the interface roughness influences light transmission, work function of the electrodes, and homogeneity of the current density. Yet, establishing precise relations between these parameters and device operation is presently limited by the lack of methods for in-situ structural and compositional analysis of as-prepared devices. Hence, techniques that allow the nature of devices to be assessed directly after processing or after operation under working conditions are of profound interest.

As an example for such analysis, we selected bulk-heterojunction photovoltaic cells in which the photoactive layer consists of a blend of a conjugated polymer as an electron donor and a C_{60} derivative as electron acceptor.[2] In these blends the intimate mixing of donor and acceptor creates a large interface, which promotes charge generation after photoexcitation because exciton dissociation occurs preferentially at the donor–acceptor interface. On the other hand, phase segregation of donor and acceptor into a bicontinuous network is thought to enhance transport of both holes and electrons. Recently, power conversion efficiencies exceeding 2.5 % under AM1.5 illumination have been reported for bulk-heterojunction cells in which the active layer is a 1:4 wt.-% mixture of poly[2-methoxy-5-(3′,7′-dimethyloctyloxy)-1,4-phenylenevinylene] (MDMO-PPV) and (1-(3-methoxycarbonyl)propyl-1-phenyl-[6,6]-methanofullerene) (PCBM).[3] These solar cells (Fig. 1) are prepared using a glass substrate covered with a transparent anode of indium tin oxide (ITO) on which a transparent conducting polymer layer poly(ethylene dioxythiophene):poly(styrene sulfonate) (PEDOT:PSS) is applied by spin coating. Subsequently, the photoactive layer is spin cast from a solution of the two components in an organic solvent. On top of this stack an Al cathode is applied by thermal deposition in vacuum, on occasion after applying a sub-nanometer interfacial layer of LiF.

With regard to these solar cells, even elementary questions regarding the integrity of interfaces in subsequent processing

[*] Prof. R. A. J. Janssen, J. K. J. van Duren
Laboratory of Macromolecular and Organic Chemistry
Eindhoven University of Technology
P.O. Box 513, NL-5600 MB Eindhoven (The Netherlands)
E-mail: r.a.j.janssen@tue.nl

Dr. J. Loos
Eindhoven Polymer Laboratories and Dutch Polymer Institute
Eindhoven University of Technology
P.O. Box 513, NL-5600 MB Eindhoven (The Netherlands)

Dr. F. Morrissey
FEI company
P.O. Box 80066, NL-5600 KA Eindhoven (The Netherlands)

C. M. Leewis, K. P. H. Kivits, Dr. L. J. van IJzendoorn
Centre for Plasmaphysics and Radiation Technology
Department of Applied Physics, Eindhoven University of Technology
P.O. Box 513, NL-5600 MB Eindhoven (The Netherlands)

Dr. M. T. Rispens, Prof. J. C. Hummelen
Stratingh Institute and Materials Science Centre, University of Groningen
Nijenborgh 4, NL-9747 AG Groningen (The Netherlands)

[**] This work was financially supported by the Dutch Ministry of Economic Affairs, the Ministry of Education, Culture and Science, and the Ministry of Housing, Spatial Planning, and the Environment through the E.E.T. program (EETK97115).

  1616-301X/02/1010-0665 $ 17.50+.50/0

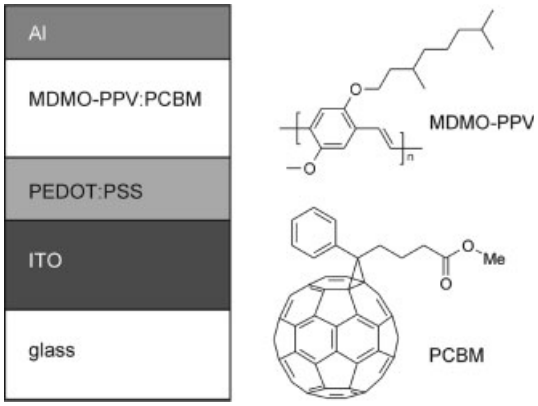

Fig. 1. Schematic layer configuration of the bulk-heterojunction photovoltaic cell and the structures of MDMO-PPV and PCBM.

steps, the possible diffusion or concentration profiles of electrode metal species into the active layers, and the question whether a spontaneous stratification (phase separation in layers) of donor and acceptor occurs, remain unanswered up to now. Here we report the use of transmission electron microscopy (TEM) and cryogenic Rutherford backscattering spectrometry (RBS) to assess these questions.

2. Results and Discussion

2.1. Electron Microscopy

To investigate details of the layer morphology, thin cross sections of a working solar cell device were prepared using the focused ion beam technique (FIB).[4,5] To prepare cross-sectional samples for TEM we used a focused ion beam (FIB) to prepare a thin $12 \times 3.5 \times 0.3\ \mu m^3$ slab from a fully processed polymer photovoltaic cell (i.e., glass/ITO/PEDOT:PSS/MDMO-PPV:PCBM/Al). FIB was then used to thin part of the specimen to approximately 100 nm. The TEM picture obtained from this cross section of the photovoltaic cell (Fig. 2) shows no visible damage to the layers and reveals various features. First, the thickness of the individual layers is readily obtained from the cross section: 155 nm ITO; 70 nm PEDOT:PSS; 160 nm MDMO-PPV:PCBM; and 70 nm aluminum. These values are consistent with the thickness of the layers determined using a surface profiler within an accuracy of 5 nm. At the interface of the photoactive MDMO-PPV:PCBM layer and the Al electrode a thin layer can be recognized, which has been identified using dual-beam dynamic time-of-flight secondary-ion mass spectrometry (TOF-SIMS) to be Al_2O_3, formed during thermal evaporation by reaction of aluminum with residual water at the polymer surface and in the gas phase.[6] Likewise, a ≈ 20 nm SiO_2 layer deposited on the glass surface can be seen in this picture. TEM also gives an impression of the roughness of the different interfaces. Both the PEDOT:PSS and the MDMO-PPV:PCBM layers are rather smooth while the ITO and the thermally evaporated Al have a larger roughness. This conclusion is corroborated by AFM measurements of the different surfaces measured at different stages during device preparation in four separate experiments (Fig. 3). The correspondence of the appearance of interfaces inferred from TEM and AFM, shows that subsequent processing steps do not significantly deteriorate layers or interfaces that were applied in previous steps.

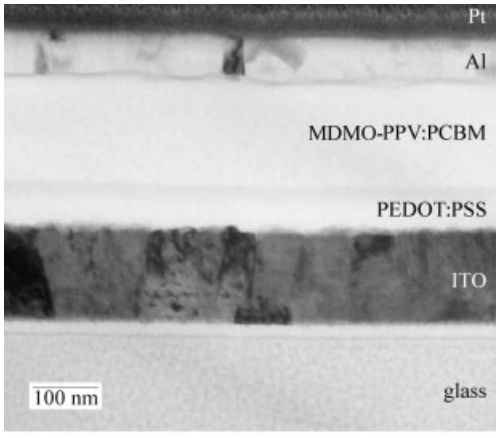

Fig. 2. TEM image of a ≈ 100 nm thick slab of a polymer solar cell consisting of a stack of glass/ITO/PEDOT:PSS/MDMO-PPV:PCBM (1:4 wt.-%)/Al.

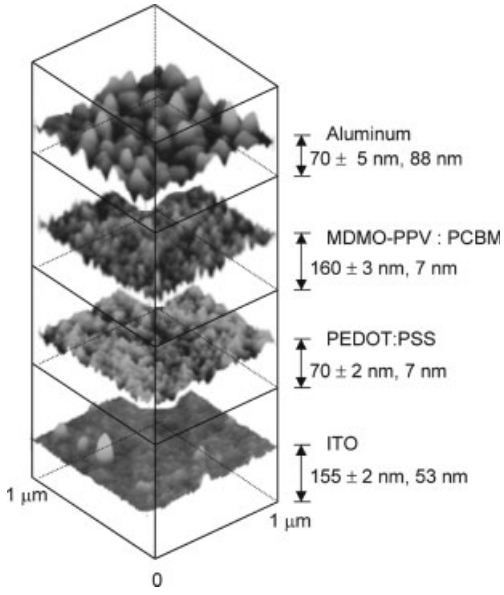

Fig. 3. AFM images of the surfaces of the different layers of a glass/ITO/ PEDOT:PSS/MDMO-PPV:PCBM (1:4 wt.-%)/Al solar cell. For each layer the thickness as determined by a surface profiler, the rms roughness of $1 \times 1\ \mu m^2$ area, and the peak-to-peak variations as determined by AFM are indicated in the graph. Both polymer layers are rather smooth and flat, the ITO is smooth, but contains spikes (see feature at the lower left corner), and the Al surface is much more rough.

2.2. In and Al Diffusion Analyzed by RBS

Cryogenic (≈ 30 K) RBS enables depth profiling of the elemental composition in the sample without the use of sputtering. For samples containing polymers, the cryogenic temperature during analysis is required in order to trap the radicals and small molecules formed by bond cleavage when the He ions

  1616-301X/02/1010-0666 $ 17.50+.50/0

pass through the film. Without cooling, small volatile molecules that escape from the material disrupt the sample structure and may even lead to gas bubbles trapped under the Al cathode.[7] Note that after the analysis, upon warm-up, the trapped radicals react and the small molecules still escape, disrupting the solar cell, which does no longer function. The RBS spectra (measured with 2 MeV He ions) show the energy distribution of the scattered projectiles. This energy depends on the masses of the projectile and scattering atom, the scattering geometry (depicted in Fig. 4A), and, moreover, to the depth at which the scattering atom is located. By carefully choosing the scattering angle θ and the angle between the incoming beam and the sample surface α, overlap of signals of different atoms can be circumvented. Both concentration depth profiles (resolution typically 10 nm) in separate layers as well as layer-to-layer diffusion can be determined. The RBS measurements are simulated using the RUMP code,[8] which provides the atomic composition and the thickness of the layer.

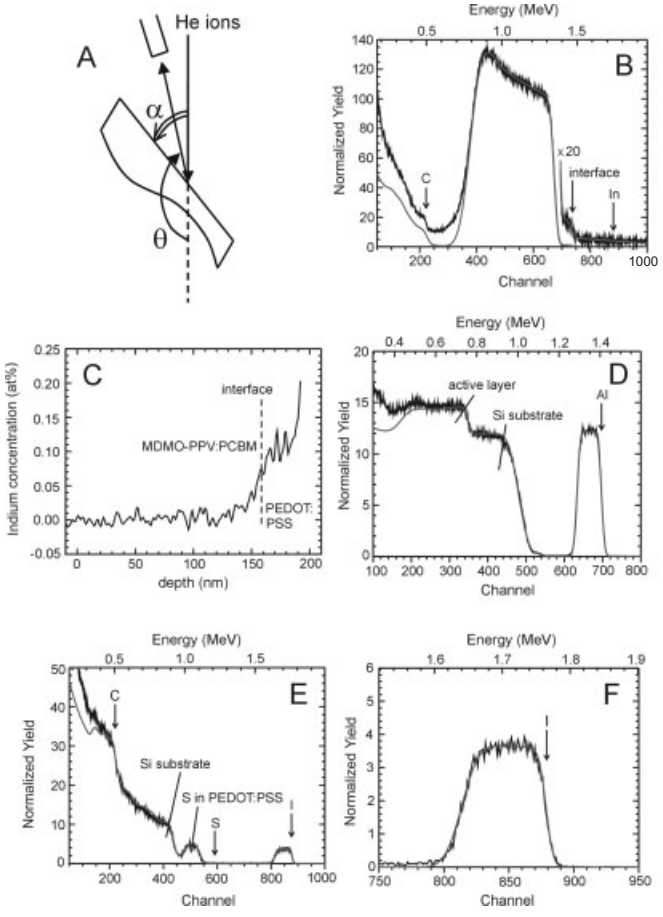

Fig. 4. RBS spectra (black) and their RUMP simulations (gray). The arrows indicate the energies that correspond to elements located at the surface. A) RBS scattering geometry. B) A glass/ITO/PEDOT:PSS/MDMO-PPV:PCBM stack, when PEDOT:PSS was dried at 150 °C for 2 min. RBS geometry: $\alpha = 165°$ and $\theta = 170°$. The simulation shows that indium diffusion is detected up to the interface between PEDOT:PSS and MDMO-PPV:PCBM. C) The indium depth profile calculated from the RBS spectrum in B assuming an atomic density of 1.3×10^{23} at. cm^{-3}. The indium concentration in the PEDOT:PSS is 0.1 ± 0.02 at.-% (corresponding to $1.3 \pm 0.3 \times 10^{20}$ at. cm^{-3}) in the PEDOT:PSS film. D) A Si/MDMO-PPV:PCBM/Al sample, when Al was deposited at a rate of 1 nm s^{-1}, analyzed at a geometry of $\alpha = 90°$ and $\theta = 100°$. E) A glass/PEDOT:PSS/MDMO-PPV:I-PCBM (1:3 wt.-%) stack, analyzed at a geometry of $\alpha = 15°$ and $\theta = 170°$. MDMO-PPV:I-PCBM (1:3 wt.-%) was spin coated at 60–65 °C from *o*-xylene. F) Enlargement of the I profile of graph (E).

The indium diffusion into the PEDOT:PSS and MDMO-PPV:PCBM layers was investigated for a glass/ITO/PEDOT:PSS/MDMO-PPV:PCBM sample for two different drying processes of the PEDOT:PSS layer, i.e., heating the substrate after spin coating on a hot plate for 1 min at 100 °C or 2 min at 150 °C. The annealing removes residual water from the PEDOT:PSS layer, which otherwise may cause etching of ITO via protonation in the acidic environment of the sulfonic acid functional groups of PEDOT:PSS.[9] The results are shown in Figures 4B and 4C. The composition of the MDMO-PPV:PCBM layer, calculated based on the used weight ratio (1:4) (63.0 at.-% C, 34.1 at.-% H, and 2.9 at.-% O), was used in the RUMP simulations. The large peak between 0.7 and 1.4 MeV corresponds to the indium in the ITO layer (Fig. 4B). Scattered He projectiles with an energy between approximately 1.4 MeV and the indium surface energy show indium diffusion into the PEDOT:PSS layer. Drying for only 1 min at 100 °C results in indium in the PEDOT:PSS layer with a concentration of 1 ± 0.1 at.-% ($1.3 \pm 0.1 \times 10^{21}$ at. cm^{-3}). After drying for 2 min at 150 °C, the indium concentration in the PEDOT:PSS is significantly reduced. The indium depth profile given in Figure 4C reveals an indium concentration of 0.1 ± 0.02 at.-% ($1.3 \pm 0.1 \times 10^{20}$ at. cm^{-3}) in the PEDOT:PSS layer up to the interface with MDMO-PPV:PCBM. The background visible in the spectra of Figure 4B between the In peak and the C peak of the active layer is due to multiple scattering in the ITO layer (which is not incorporated in the simulation). The results are consistent with the fact that residual water promotes the diffusion of In.

Al diffusion into the active layer was investigated for Si/MDMO-PPV:PCBM/Al stacks for Al deposition rates of 1 and 10 nm s^{-1}. In these experiments a silicon substrate was chosen instead of glass/ITO to avoid overlap of the Al peak by Ca and In from the glass and ITO, respectively. The peak between 1.25 and 1.40 MeV for a deposition rate of 1 nm s^{-1} in Figure 4D corresponds to the Al layer. Aluminum diffusion into the MDMO-PPV:PCBM film might be observed at energies just below 1.25 MeV. For both deposition rates, however, no aluminum was detected in the active layer above the detection limit of 0.1 % and since the RBS spectra of both samples are identical, only the spectrum of 1 nm s^{-1} is presented (Fig. 4D). For both deposition rates, the sample can be simulated by RUMP with oxygen only in the first few nanometers. The roughness of the interface between the polymer layer and Al used in the RUMP simulations is less than 15 % of the total polymer film thickness.

2.3. Stratification in Phase Separation

Stratification of donor and acceptor in MDMO-PPV and PCBM has been described by making use of the temperature-dependent solubility of MDMO-PPV in *o*-xylene by first spin coating MDMO-PPV from a hot solution and subsequently spin coating PCBM at room temperature.[10] These stratified

  1616-301X/02/1010-0667 $ 17.50+.50/0

layers have a diffuse interface and resulted in higher fill factors and energy-conversion efficiencies.[10] However, the possibility that spontaneous stratification of MDMO-PPV and PCBM occurs or that a concentration profile is formed in the photoactive layer, has not been tested.

We used RBS to determine the concentration depth profile of PCBM in the active layer of the photovoltaic cell. For this purpose I-PCBM, an iodinated fullerene derivative (Fig. 5), was used to distinguish between PCBM and the polymer in the RBS spectra. Iodine serves as a label of the PCBM and thereby resolves the problem of overlapping C, H, and O-peaks of PCBM and MDMO-PPV in the RBS spectrum. The synthesis of I-PCBM started from easily accessible 4-chlorocarbonyl butyric acid methyl ester (**1**) (Fig. 5).[11] Friedel–Crafts acylation of iodobenzene yielded the corresponding keto ester as a mixture of the 4-I-phenyl (**2a**) and 2-I-phenyl (**2b**) isomers, which were transformed into the corresponding *p*-tosylhydrazones and purified by column chromatography to yield pure **3a**. Subsequently, I-PCBM was prepared by heating the anion of **3a** in the presence of [60]fullerene in *o*-dichlorobenzene (ODCB) at 80–90 °C to give fulleroid **4a**, together with methanofullerene **4b**, higher adducts, and [60]fullerene.[12] After column chromatography, the mixture of **4a** and **4b** was photoisomerized quantitatively to **4b** in ODCB. Final purification was done by column chromatography, affording pure **4b** (I-PCBM) as a brown powder in 24 % overall yield (four steps), starting from **3a**. I-PCBM was fully characterized using ^{1}H NMR, ^{13}C NMR, UV-vis, FT-IR, and matrix-assisted laser desorption ionization time-of-flight (MALDI-TOF) mass spectrometry. The UV-vis spectrum of I-PCBM and the first redox potential as determined by cyclic voltammetry are identical to that of PCBM.

The iodine distribution in the active layer has been investigated for several glass/PEDOT:PSS/MDMO-PPV:I-PCBM samples, spin cast from *o*-xylene (ratio MDMO-PPV:I-PCBM of 4:1, 1:3, and 1:4, w/w) at 60–65 °C. The RBS spectrum and RUMP simulation of a sample with MDMO-PPV and I-PCBM (1:3 wt.-%) is shown in Figures 4E and 4F. The iodine surface energy, 1.77 MeV, is shown as well as the edges of S (PEDOT:PSS), Si (glass), and C (MDMO-PPV). The enlargement of the I RBS spectrum in Figure 4F shows a homogeneous iodine concentration in the active layer corresponding to a concentration of $5.0 \pm 0.2 \times 10^{-3}$ at.-%. To explain the slope of the I signal on the low-energy side, a roughness of 15 nm had to be introduced for the interface between PEDOT:PSS and the active layer. The absence of a strong tendency for MDMO-PPV and I-PCBM to give stratification did not change when different weight ratios (MDMO-PPV:I-PCBM 4:1, 1:3, or 1:4 wt.-%) were analyzed.

Despite the structural similarity of I-PCBM and PCBM, they may behave differently when mixed with MDMO-PPV. In this respect the present study cannot give an unambiguous conclusion with respect to possible stratification in MDMO-PPV:PCBM layers. We noted that layers of MDMO-PPV with I-PCBM layers have a larger surface roughness than layers with PCBM. This suggests that the (lateral) phase separation in layers of MDMO-PPV with PCBM is less than that with I-PCBM. Based on this result we believe that absence of stratification observed by RBS for MDMO-PPV:I-PCBM, also pertains to MDMO-PPV:PCBM thin films.

3. Conclusions

Polymer photovoltaic cells and their multiple layer substructures have been analyzed using TEM of cross sections and cryogenic RBS in terms of interface roughness and interlayer diffusion of electrode materials. We have shown that, using FIB, cross sections of fully processed photovoltaic cells can be made, which reveal information on the thickness of the layers and on the roughness and nature of the interfaces. The results from TEM corroborate with those from AFM and dynamic TOF-SIMS measurements, and indicate that no significant damage occurs in the preparation of the cross sections. RBS revealed that diffusion of Al and In into the polymer layers is minor directly after preparation, provided that appropriate annealing is performed. The RBS technique has also been used to show that in MDMO-PPV:I-PCBM layers no spontaneous stratification of the two components occurs during spin coating. It must be noted that this conclusion cannot be taken as a universal property for bulk-heterojunction polymer solar cells because the structure of the active layer is subject to changes via processing conditions (e.g., nature of the solvent, and drying conditions) and the specific compounds used (e.g., type of polymer and C_{60} derivative).

Future studies will be directed to use both TEM and RBS to analyze cells that have been operating under working conditions and check for integrity of interfaces (possible delamination) and diffusion of ions due to higher temperatures or the presence of an electric field.

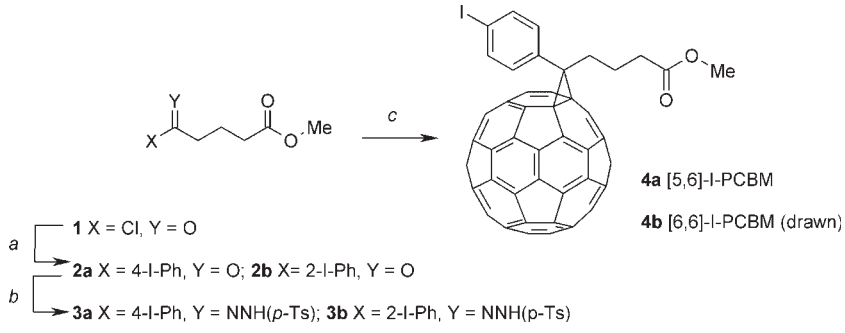

Fig. 5. Synthesis of I-PCBM (**4b**). a) PhI, $AlCl_3$, 0 °C, 64 h., 59 % (mixture of isomers **2a** and **2b**). b) $TosNHNH_2$, MeOH, Δ, 6 h., 60 %. c) 1: NaOMe, pyridine; 2: [60]fullerene, ODCB, 65 °C, 16 h., 3: *hν*, ODCB, 500 W flood lamp, 2 h., 24 % (4 steps, starting from **3a**).

4. Experimental

Photovoltaic Cells: ITO covered glass substrates were cleaned by ultrasonic treatment in acetone, rubbing with soap, rinsing with demineralized water, refluxing with isopropanol, and finally UV ozone treatment. Poly(ethylene dioxythiophene):poly(styrene sulfonate) (PEDOT:PSS,

  1616-301X/02/1010-0668 $ 17.50+.50/0

ADVANCED FUNCTIONAL MATERIALS

Bayer AG) was spin coated from an aqueous dispersion under ambient conditions on the cleaned substrates and the layer was dried by annealing the substrate on a hot plate at 100 °C for 1 min, unless stated otherwise. Subsequently a MDMO-PPV:PCBM (1:4 wt.-%) layer was spin coated from *o*-xylene solution at ≈ 60 °C and the sample was transferred to a N_2 atmosphere glove box. Finally an aluminum back electrode was deposited by thermal evaporation under vacuum (5×10^{-6} mbar, 1 ppm O_2, and < 1 ppm H_2O). The total device consists of the following layer thickness: 155 nm ITO; 70 nm PEDOT:PSS; 160 nm active layer, and 70 nm Al, as determined with a Tencor P-10 surface profiler.

Focused Ion Beam and Transmission Electron Microscopy: The gallium (Ga) ion beam of the used FIB (Strata FIB200, FEI Company, The Netherlands) has a beam size in the order of 10 nm and is used to mill through the device. After coarse milling the sides of the cross section are polished by the beam using a very low beam current. For transmission electron microscope (TEM) investigations the cross-sections were transferred on copper grids coated with a carbon film consisting of woven-mesh-like holes of different sizes and shapes. Details of the complete preparation procedure have been described elsewhere [13]. TEM was performed using a Jeol 2000FX operated at 80 kV.

Rutherford Backscattering Spectrometry: Samples for RBS of approximately 1.1×2.5 cm^2 were mounted on the sample holder in the glove box. A cryo paste was used to improve heat conduction between the sample and sample holder during the cryogenic measurements. The samples were transported to the cryogenic RBS setup in a sealed holder in N_2 atmosphere and transferred to the analysis chamber by a load lock, without exposure to air. The RBS measurements were performed using a 2 MeV He^+ beam from the 2–30 MeV AVF cyclotron at Eindhoven University of Technology using a current of typically 10 nA. Using a solid-state detector with a solid angle of 2.5 mrad, the count rate was limited to approximately 1000 counts s^{-1} minimizing pile up. The size of the beam spot is 1×1 mm^2. The angle of incidence of the beam relative to the sample surface could be adjusted between 0° and 90°, while the RBS detector could be moved to select any scattering angle between 0° and 180°. The simulations of the RBS measurements were performed with the RUMP code [8]. For accurate RUMP simulations it was necessary to determine the composition of the glass and ITO in separate experiments. The composition of the glass was determined with the beam directed along the surface normal ($\alpha = 90°$ and $\theta = 165°$) and gave 62.0 at.-% O, 25.6 at.-% Si, 9.6 at.-% Na, and 2.8 at.-% Ca. The composition of ITO, determined at the same geometry equals 61 at.-% O and 39 at.-% In. The Sn fraction was disregarded because In and Sn were indistinguishable in the RBS measurements and the Sn fraction in ITO is small (1–10 %) [14]. In the simulations the composition of the PEDOT:PSS was assumed to be 43 at.-% C, 34 at.-% H, 17 at.-% O, and 5 at.-% S [15].

*4-(Iodobenzoyl)butyric Acid Methyl Ester (**2**, Mixture of Isomers)*: 4-Chlorocarbonyl-butyric acid methyl ester [11] (**1**, 4.94 g; 30 mmol) was dissolved in iodobenzene (50 mL), and portions of aluminum chloride (8.0 g; 60 mmol) were added (0 °C). After the addition was complete, the reaction was allowed to stir at 0 °C for 64 h. The now heterogeneous mixture was poured on ice (200 g) while stirring (CAUTION!, vigorous reaction). The resulting mixture was extracted with ether (4×200 mL). The combined organic layers were washed with diluted aqueous sodium dithionite (200 mL), water (200 mL), sodium carbonate (dil. aq., 200 mL), and brine (200 mL). The organic phase was dried over sodium sulfate, filtered, and evaporated in vacuo. The remaining yellow oil was purified by bulb-to-bulb distillation ($p \sim 4$ mm Hg, $T = 180$–200 °C). Crystallization from cyclohexane gave a mixture of 4-(4-iodobenzoyl)butyric acid methyl ester (**2a**) and 4-(2-iodobenzoyl)butyric acid methyl ester (**2b**) (5.88 g, 17.6 mmol, 59 %, ratio 79(*para*):21(*ortho*)) that was used in the subsequent reaction; an analytical sample of **2a** was obtained by column chromatography (Si gel; toluene). **2a**: mp.: 63.8–64.8 °C; ^{1}H NMR ($CDCl_3$, 300 MHz): δ [ppm]: 7.86–7.80 (m, 2H), 7.70–7.64 (m, 2H), 3.68 (s, 3H), 3.01 (t, J=7.2, 2H), 2.44 (t, J=7.2), 2.06 (p, J=7.2); ^{13}C NMR ($CDCl_3$, 75 MHz): δ [ppm]: 198.59, 173.59, 137.89, 135.99, 129.40, 100.99, 51.58, 37.32, 32.97, 19.18; FTIR (KBr): 1735 (s), 1677 (s); HRMS (EI$^+$) Calcd. for $^{12}C_{12}H_{13}IO_3$ (M^+): $m/z = 331.991$. Found: $m/z = 331.992$. Anal. Calcd. for $C_{12}H_{13}IO_3$: C, 43.40; H, 3.95; I, 38.21; Found: C, 43.55; H, 3.76; I, 38.08.

*4-(4-Iodobenzoyl)butyric Acid Methyl Ester p-Tosyl Hydrazone (**3a**)*: A mixture of 4-(4-iodobenzoyl)butyric acid methyl ester (**2a**) and 4-(2-iodobenzoyl)butyric acid methyl ester (4.98 g, 15 mmol, ratio 79:21) and toluene-4-sulfonic acid hydrazide (9.00 g, 52 mmol, 3.5 equiv) was dissolved in methanol (25 mL). The mixture was heated under reflux for 5.5 h, and subsequently allowed to reach room temperature overnight. The precipitate was filtered, washed with methanol and dried. ^{1}H NMR showed that a mixture of product **3a** and 4-(2-iodobenzoyl)-butyric acid methyl ester *p*-tosyl hydrazone (**3b**) was formed in a ratio of 79:21. Separation was done by column chromatography (Si gel; ether/cyclohexane = 1:1), giving pure **3a** (5.49 g, 60 %); mp.: 123.1–125.6 °C; ^{1}H NMR ($CDCl_3$, 300 MHz): δ [ppm]: 9.29 (br s, 1H), 7.90 (d, J=8.1, 2H), 7.67 (d, J=8.4, 2H), 7.38 (d, J=8.7, 2H), 7.30 (d, J=7.8, 2H), 3.81 (s, 3H), 2.61–2.56 (m, 2H), 2.41 (s, 3H), 2.36–2.32 (m, 2H), 1.71–1.60 (m, 2H); ^{13}C NMR ($CDCl_3$, 75 MHz): δ [ppm]: 174.74, 152.47, 143.84, 137.56, 135.88, 135.67, 129.50, 127.88, 127.80, 95.74, 52.40, 31.96, 25.59, 21.57, 20.80; FTIR (KBr): 3115 (s), 1707 (s), 1368 (s), 1231 (s), 1171 (s), 1071 (m); HRMS Calcd. for $C_{19}H_{21}IN_2SO_4$ 500.027, found 500.028. Anal. Calcd. for $C_{19}H_{21}IN_2SO_4$: C, 45.61; H, 4.23; I, 25.36; N, 5.60; S, 6.41; Found: C, 45.83; H, 4.28; I, 25.06; N, 5.61; S, 6.40.

*I-PCBM (**4a**)*: 4-(4-Iodobenzoyl)butyric acid methyl ester *p*-tosyl hydrazone (**3a**, 555 mg, 1.11 mmol) was dissolved in pyridine (15 mL, dry). Sodium methoxide (59.4 mg, 11.0 mmol) was added and the mixture was stirred for 30 min. A solution of [60]fullerene (720 mg, 1.00 mmol) in *o*-dichlorobenzene (ODCB, 50 mL, HPLC grade) was added and the mixture was stirred overnight, maintaining the temperature at 60–70 °C. After cooling the mixture to room temperature, the ODCB was removed at the rotary evaporator until approx. 10 mL was left. The remaining mixture was brought on top of a silica gel column (CAUTION! Pour column in toluene/cyclohexane = 1:1 and pre-treat the column with CS_2, because mixing silica gel and CS_2 directly generates enough heat to ignite the CS_2). The column was eluted with CS_2 until all [60]fullerene (259 mg, 36 %) was removed. An isomeric mixture of products was eluted with toluene/cyclohexane = 1:1. The solvent was removed in vacuo. The mixture of [5,6] and [6,6] compounds (**4a** isomers and **4b**, 475 mg) was dissolved in ODCB (200 mL) and irradiated with a 500 W sodium lamp, while cooling, until complete conversion to the methanofullerene (approx. 2 h). After the removal of the solvent the product was purified by column chromatography (Si gel; toluene/cyclohexane = 1:2). The fractions containing pure compound were collected, and the solvent was removed in vacuo. The product was redissolved in a minimal amount of ODCB. Methanol was added and the mixture was centrifuged and decanted (3×). The pellet obtained was dried overnight in a vacuum oven ($T = 50$ °C), obtaining pure I-PCBM (**4b**, 366 mg, overall 24 %); mp.: > 300 °C; ^{1}H NMR (CS_2, 500 MHz): δ [ppm]: 8.00 (d, J=8.5, 2H), 7.80 (d, J=8.5, 2H), 3.76 (s, 3H), 3.03–3.00 (m, 2H), 2.61 (t, J=7.3, 2H), 2.31–2.24 (m, 2H); ^{13}C NMR (CS_2, 125 MHz): δ [ppm]: 171.08, 147.83, 147.04, 145.46, 145.03, 144.99, 144.93, 144.74, 144.61, 144.55, 144.50, 144.33, 144.02, 143.56, 142.95, 142.88, 142.84, 142.81, 141.98, 141.96, 141.95, 141.86, 140.90, 140.69, 138.00, 137.55, 137.52, 136.13, 133.57, 95.19, 79.09, 51.03, 50.98, 33.46, 33.44, 22.50; FTIR (KBr): 1736 (s), 525 (s); UV-vis (toluene): 331 ($\varepsilon = 44\,700$), 433 (2770), 496 (1660), 695 (257); MALDI-TOF MS: Calcd. for $^{12}C_{72}H_{13}IO_2$ (M^+): $m/z = 1036.0$. Found: $m/z = 1036.3$; Anal. Calcd. for $C_{72}H_{13}IO_2$: C, 83.41; H, 1.26; I, 12.24; Found: C, 83.27; H, 1.48; I, 12.12.

Received: April 13, 2002
Final version: July 10, 2002

[1] R. H. Friend, R. W. Gymer, A. B. Holmes, J. H. Burroughes, R. N. Marks, C. Taliani, D. D. C. Bradley, D. A. Dos Santos, J. L. Brédas, M. Lögdlund, W. R. Salaneck, *Nature* **1999**, *397*, 121.
[2] G. Yu, J. Gao, J. C. Hummelen, F. Wudl, A. J. Heeger, *Science* **1995**, *270*, 1789.
[3] S. E. Shaheen, C. J. Brabec, F. Padinger, P. Fromherz, J. C. Hummelen, N. S. Sariciftci, *Appl. Phys. Lett.* **2001**, *78*, 841.
[4] L. A. Giannuzzi, F. A. Stevie, *Micron* **1999**, *30*, 197.
[5] M. W. Phaneuf, *Micron* **1999**, *30*, 277.
[6] C. W. T. Bulle-Lieuwma, W. J. H. van Gennip, J. K. J. van Duren, P. Jonkheijm, R. A. J. Janssen, J. W. Niemantsverdriet, *Appl. Surf. Sci.* **2002**, in press.
[7] M. P. de Jong, L. J. van IJzendoorn, M. J. A. de Voigt, *Nucl. Instrum. Methods Phys. Res. B* **2000**, *161*, 207.
[8] L. R. Doolittle, *Nucl. Instrum. Methods Phys. Res. B* **1985**, *9*, 344.
[9] M. P. de Jong, L. J. van IJzendoorn, M. J. A. de Voigt, *Appl. Phys. Lett.* **2000**, *77*, 2255.
[10] L. C. Chen, D. Godovsky, O. Inganäs, J. C. Hummelen, R. A. J. Janssen, M. R. Andersson, *Adv. Mater.* **2000**, *12*, 1367.
[11] J. Cason, *Org. Synth., Coll. Vol. III* **1955**, 171.
[12] J. C. Hummelen, B. W. Knight, F. LePeq, F. Wudl, J. Yao, C. L. Wilkins, *J. Org. Chem.* **1995**, *60*, 532.
[13] J. Loos, J. K. J. van Duren, R. A. J. Janssen, F. Morrissey, *Polymer* **2002**, in press.
[14] M. P. de Jong, *Ph.D. Thesis*, Eindhoven University of Technology **2000**.
[15] A. J. Heeger, A. N. Aleshin, S. R. Williams, *Synth. Met.* **1998**, *94*, 173.

  1616-301X/02/1010-0669 $ 17.50+.50/0